PDTC suppression of CCR7 affects EMT in the AGS gastric carcinoma cell line

Yuan Jiang
Department of Cancer Immunology, Fudan Medical University, Liang Laboratory, Shanghai, China

Abstract

Previous research has demonstrated that a significant correlation exists between the expression of chemokine co-receptor 7 (CCR7) and the onset of epithelial mesenchymal transition (EMT) in gastric carcinoma cells (Mashino et al. 2002). To further investigate the role of CCR7 in inducing EMT, we studied the AGS line of gastric carcinoma and one of its known inhibitors, pyrrolidine dithiocarbamate (PTDC). PDTC also inhibits the transcription factor NF-κB, which has been previously demonstrated to be highly involved in EMT induction (Zhou et al. 2010). After culturing, AGS cells were divided into 5 PDTC dosage groups: 0 (control), 20, 50, 100 and 200 mg/L. Wound-healing assays quantified migratory abilities between dosage groups and demonstrated that PDTC treatment affected cell migration, though not in a linear fashion. Morphology assays concluded that PDTC treatment did not significantly alter morphodiversity between dosage groups, though EMT-related transformations were largely accountable for morphology changes *within* groups. Western blot analysis demonstrated relative consistency in expression of CCR7 and standard EMT markers across the board, suggesting PDTC did may not have been an effective inhibitor. Finally, an immunohistochemistry assay (IHC) performed on clinical tumor and non-tumor samples demonstrated increased proliferation of CCR7+ tumor cells and decreased CCR7+ immune effector cells in tumor samples.

Introduction

Every year, over 20,000 people in the U.S. are diagnosed with gastric carcinoma while another 11,000 people die from it (Crew and Neugut 2006). In parts of East Asia, it is even more frequent; for example, gastric carcinoma is the most common type of cancer found in South Korea, and accounts for over 20% of annual deaths (Lee et al. 2002). At present, it is the second leading cause of cancer-related deaths in the world as most patients that are diagnosed present with late stage cancer progression (Crew and Neugut 2006). Due to this phenomenon, it is critical to better study and understand the biological factors that contribute to gastric carcinoma's high lethality among patients.

Gastric carcinoma is also known as cancer of the stomach. The stomach wall consists of five layers: mucosa, submucosa, muscle layer, subserosa, and serosa. Gastric carcinoma typically originates in the innermost layer, the mucosa, and then penetrates into the other layers, eventually reaching the blood and lymphatic system (Crew and Neugut 2006). In extreme cases, tumors that form can penetrate the serosa and invade nearby organs such as the liver or intestines. Most cancerous cells can be found adjacent to lymph nodes near the stomach. As tumors spread to more distal areas of the body, treatment and full recovery become increasingly challenging (Carl-McGrath et al. 2007).

Gastric carcinoma is also known to progress in stages; in stage 0, the cancer is only found in the mucosa while in stages I and II, it has already invaded into the submucosa or subserosa (Slowik 2012). In stages III and IV, the tumor proceeds to invade into lymph nodes and nearby organs. During the early stages of gastric carcinoma, surgery is the most commonly used protocol for removing cancerous tissue, but once the tumor has metastasized to other organs, surgical methods and full recovery are often no longer options for many patients (Crew and Neugut 2006). In addition, many patients do not recognize symptoms of the disease until it has progressed beyond control (Carl-McGrath et al. 2007). Due to the fast spreading nature of gastric

carcinoma, it is thus important to examine and understand the mechanisms by which metastasis is induced at the molecular level.

In the present study, we will be investigating the role of CCR7 and one of its inhibitors, pyrrolidine dithiocarbamate (PTDC), in inducing epithelial-mesenchymal transition (EMT) and metastasis in AGS gastric carcinoma cells. In specific, we will be studying gastric adenocarcinoma, a malignant epithelial tumor that undergoes EMT to metastasize to other stomach layers and organs (Carl-McGrath et al. 2007). AGS cells present with a relatively high quantity of CCR7 as compared to other gastric carcinoma lines and thus serve as an optimal study focus for our project (Kwak et al. 2005). CCR7 is also expressed in a variety of immune effector and cancerous cells, and thus has been hypothesized to be significantly involved in lymph node metastasis (Kwak et al. 2005).

First and foremost, CCR7 is a chemokine receptor that is part of the G protein-coupled receptor family and is commonly expressed in immune effector cells such as dendritic cells and T-cells (Zhou et al. 2010). Past research has also shown that CCR7 is highly correlated with the onset of EMT in gastric carcinoma cells (Mashino et al. 2002) and is particularly responsible for tumor migration towards lymph nodes. EMT is a physiological process by which epithelial cells lose their normal cell characteristics and take on the mesenchymal stem cell phenotype, and then proceed to migrate and invade other tissues via the lymphatic vessels (Wang et al. 2013). In particular, epithelial cells lose their cell-cell adhesive properties and cell polarity, and accordingly become spindle-shaped to better accommodate their migratory abilities. Previous studies have also demonstrated that cells undergoing EMT exhibit increasing levels of calcium and actin polymerization, resulting in reorganization of their entire cytoskeletal network (Mashino et al. 2002). In losing their cell-cell adhesive properties and gaining their migratory/invasive abilities, these cells must first downregulate E-cadherin (crucial in cell adhesion) while upregulating N-cadherin. Other significant markers of EMT include vimentin, Snail1, and β-catenin. These modified cells then migrate towards lymph nodes via the lymphatic system where they can then travel to different parts of the body and generate new tumors (Xu et al. 2009). If CCR7 proves to be a critical factor in inducing EMT, possible future therapies may utilize this fact to block CCR7 expression more efficiently in hopes of delaying or suppressing cancer metastasis.

Past research has demonstrated that PDTC is heavily involved with the transcription factor NF-κB, which is also an important inducer of EMT (Maier et al. 2010). PDTC has also been shown to inhibit CCR7 in dendritic cells derived from bone-marrow (Zhou et al. 2010). However, this inhibition has only been established in the presence of secondary lymphoid tissue chemokine (SLC). Research by Zhou et al. (2010) has also suggested that PDTC may affect EMT in gastric carcinoma cells independent of the Nf-κB pathway.

In order to study the role of CCR7 in inducing EMT, we will adopt an integrative approach in which we analyze the morphological, behavioral, and molecular characteristics of EMT. Using PDTC as an inhibitor, we will investigate whether modulation in CCR7 expression affect EMT in terms of migratory ability, morphology, and molecular markers. Morphological analysis will be conducted to examine whether cells are adopting morphologies more typical of the mesenchymal phenotype (spindle-shaped) and whether PDTC treatment significantly affected cell morphology between different treatment groups. An inquiry into the behavioral components of EMT will be conducted by way of a wound-healing assay. And finally, at the molecular level, we will examine the various markers associated with EMT to confirm that the cells have undergone EMT. To study CCR7 expression in an *in vivo* setting, we will be conducting a statistical analysis to comparatively quantify the proliferation of CCR7+ tumor cells in clinical samples.

Note: Unfortunately, due to both time constraints and the fact that our shipment of CCL21 never came, we abandoned our original plan of adding CCL21 (one of CCR7's ligand) to the cells and opted to use PDTC instead. To compensate for this, we assumed that a certain level of CCl21 was already present in our cell lines and thus proceeded with our experimental design.

Methodology

Materials

All research was conducted in the Liang Laboratory in the Department of Cancer Immunology at Fudan Medical University in Shanghai, China under the supervision of Dr. Huiying Ma. Gastric carcinoma AGS cells were provided by Dr. Ma and Professor Liang. Once cultured, AGS cells were divided into 5 groups in which increasing amounts of PDTC were added to each group: 0 (control), 20, 50, 100 and 200 mg/L. For Western blot, treatment groups were further split into two time groups: PDTC incubation for 24 hours and 48 hours. Clinical gastric adenocarcinoma samples for immunohistochemistry (IHC) analysis were provided by Zhongshan Hospital in Shanghai, China.

Cell Culture

The AGS cell line was cultured in 1640 medium supplemented with 10% fetal bovine serum (FBS), 100 U/ml penicillin, and 100 Ug/ml streptomycin. The AGS cell culture was incubated in a 5% CO_2-humidified atmosphere at 37°C. The medium was changed every time the cell culture reached around 80-90% confluency. Cells were passaged four times and treated and used for experimental purposes at the fifth passage. Concentration of AGS cells were determined at 4 x 10^5 cells/mL for the wound-healing (scratch) assay and 1 x 10^5 cells/mL for western blotting.

Wound-healing/Scratch Assay

AGS cells were seeded in 6-well plates and cultured until 100% confluency. Each well was then incubated with 0 (control), 20, 50, 100, or 200 mg/mL of PTDC for 1 hour. A straight scratch was then performed by a yellow 200 µL micropipette tip. Each well was subsequently washed with PBS three times before adding fresh 1640 medium supplemented with 10% bovine serum. Images of the healing wound were then taken at regular 12-hour intervals after initial scratch. Pictures were then analyzed by computer imaging software to quantify migratory abilities by measuring percentage of wound healing at various time points.

Morphology Assay

AGS cells were seeded in individual plates and cultured until 40% confluency. Cells were then observed with electron microscopy and images were taken with imaging software. Analysis of changes in morphology was done with MorphoJ (University of Manchester, UK). Specifically, landmarks were placed on three cell images for each experimental and control group, and coordinates of the landmarks were then arranged in a dataset that was further analyzed by linear regression and principal component analysis. Wireframe and transformation grid images ranging in scale factors for each principal component was then analyzed and compared. A canonical variate analysis was then performed to test whether morphologies significantly differed between experimental groups.

Western Blot

For Western blot analysis, each experimental group was treated with either 0 (control), 20, 50, 100, or 200 mg/mL of PTDC. Each experimental group was further divided into two groups: one incubated with PDTC for 24 hours and once incubated with PDTC for 48 hours before protein harvesting. The cells were then washed with PBS, harvested by scraping and centrifuged at 12,000 rpm for 30 minutes. The cell pellets were sonicated in cold lysis buffer (EDTA-free PROPREPTM Protein Extraction Solution; iNtRON Biotechnology, Inc., Seoul, Korea) and protein concentration was then determined with a BCA protein assay kit (Pierce,

Rockford, IL, USA). Proteins were run in a variety of 6% to 12% SDS-PAGE Biorad gels at 40V and 100V for 30 and 90 minutes, respectively. The gel was then cut into sections and proteins were transferred to polyvinylidene fluoride (PVDF) membranes. Membranes were then blocked with 5% nonfat milk for 1 hour at room temperature and then incubated at 4°C overnight with 1:2000 dilutions of monoclonal primary antibodies against GAPDH (loading control; Millipore, Rockland, NY), CCR7, vimentin, N-cadherin, and E-cadherin, and Snail1 (Epitomics, Burlingame, CA). Membranes were washed with a mixture of tris-buffered saline and tween 20 (TBST) and incubated with dilutions of secondary antibodies (1:2000) for 2 hours at room temperature and then washed again. Finally, proteins were visualized and relative expression levels quantified using an enhanced chemiluminescence procedure (enhanced chemiluminescence reagent; Millipore, Billerica, MA) and imaging software ImageLab (Bio-rad, Hercules, CA).

Immunohistochemistry Assay

Gastric carcinoma tumor tissues were harvested and fixed in formaldehyde (4% buffered) followed by embedding in paraffin. 22 Samples were then processed for IHC staining. Sections were cut at a thickness of 6 µm, mounted onto slides and dried on a 37°C plate for 1 hour. To remove the paraffin wax, sections were immersed in xylene and rehydrated in decreasing concentrations of ethanol. Slides were immersed in sodium citrate buffer and heated in a microwave for 5 minutes twice, and were then allowed to cool to room temperature. After cooling, slides were immersed in 0.01M phosphate buffer solution (PBS), then a hydrogen peroxide-methanol-PBS solution, and then rinsed again in PBS. To lyse the cell membrane, slides were immersed in 0.3% triton100-x-PBS. Sections were then blocked with normal goat serum for 60 min. Subsequently, sections were stained and allowed to associate with CCR7 rabbit anti-human primary antibody (1:200; Epitomics, Burlingame, CA) overnight; this was followed by staining with goat anti-rabbit secondary antibody (1:200). To control for non-specific background staining, 8 control groups were created in which the primary antibody was not added. All sections were counterstained with Gill's hematoxylin. Immunostained tumor sections were examined by bright field microscopy and imaged by Imagelab (Bio-rad, Hercules, CA) imaging software.

Results and Discussion

Morphological Assay: Morphodiversity within PDTC dosage groups is associated with EMT

For morphological analysis, landmarks were placed on three cell images from different time points for each experimental group as shown in Figure 1. The principal component analysis returned two components that were statistically significant. Each principal component is a geometric transformation that contributes to a deviation from the average morphology as calculated by MorphoJ. Figure 2 illustrates the two principal components that were largely accountable for morphodiversity in experimental and control groups.

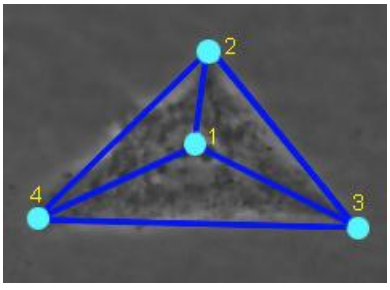

Figure 1. Cyan dots mark where landmarks were placed on cells for each image. Point 1 locates the nucleus whereas points 2, 3, and 4 mark cell pseudopodia. Typical AGS cells are trigonal and tend to cluster together. However, only stand-alone cells were analyzed for morphology. Points in the dataset were ordered by decreasing distance to the nucleus.

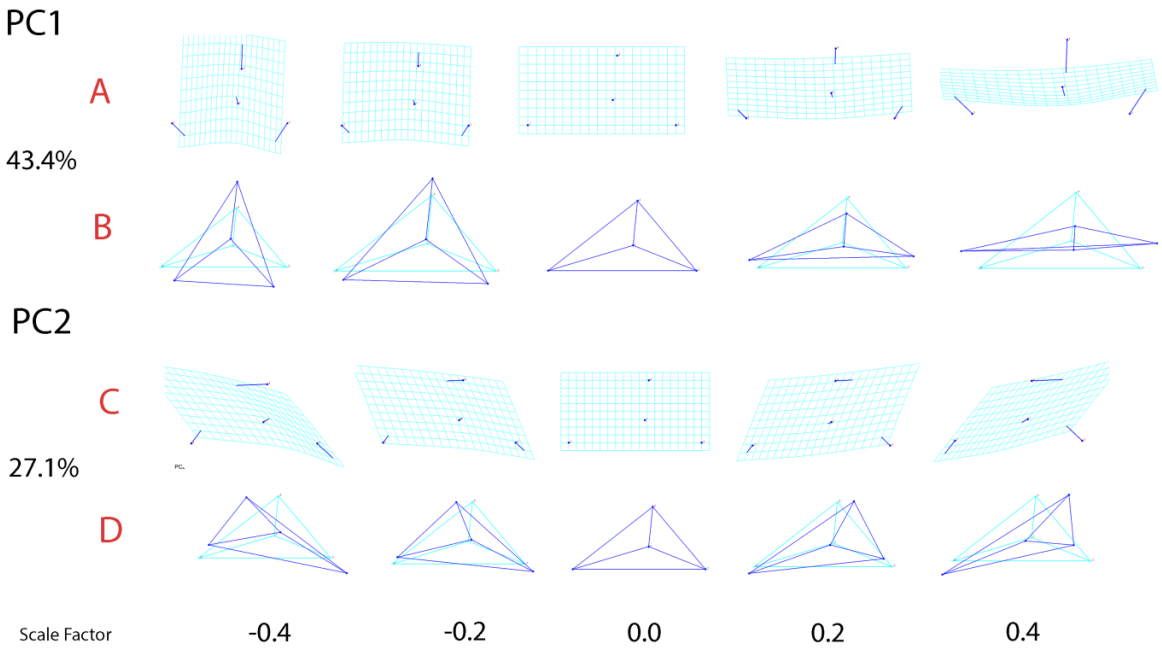

Figure 2. Principal component of morphometric analysis allows 2D visualization of geometric transformations. Wireframe diagrams and transformation grids were constructed to visualize principal components ranging in scale factor. PC1 detailed cell elongation whereas PC2 illustrated cell pseudopodia formation and orientation.

Average morphology was determined by taking the average of all coordinates, taking both distances and angles of rotation into consideration. Scale factors were associated with a particular principal geometric transformation. As Figure 2 demonstrates, 43.4% of observed morphological variance can be explained by principal component 1. PC1 is a geometric transformation corresponding to cell elongation. Centroid size was also evaluated by running a linear regression to see if scale factors were correlated with the centroid size of sample cells. The p-value obtained from the linear regression was specified at 0.87. With an alpha significance level set at 0.05, we did not have enough evidence to therefore conclude that centroid size was correlated with PC1 scale factors.

PC2 described 27.1% of morphological variance in the treatment cells alone. In particular, PC2 corresponded with pseudopodia elongation at different cell vertices. The sign for the scale factor determined the orientation of pseudopodia formation in morphospace. Notably, PC2 was not correlated with centroid size and was independent of PC1.

Finally, a canonical variate analysis was performed to evaluate between group variation. A p-value of 0.47 was obtained, and thus we were unable to conclude that there were significant morphological differences between experimental groups. Overall, principal component analysis supported our hypothesis by demonstrating that our cell morphologies were typical of cells undergoing EMT.

Wound-healing/Scratch Assay: PDTC affects cell migration

After wound-healing assay images were analyzed with Tscratch (Swiss Federal Institute of Technology, Zürich, Germany) at a threshold of 0.25, a linear regression was run on the percent of wound healing in the scratch as well as an analysis for variance (ANOVA) residuals test for significance between treatment groups.

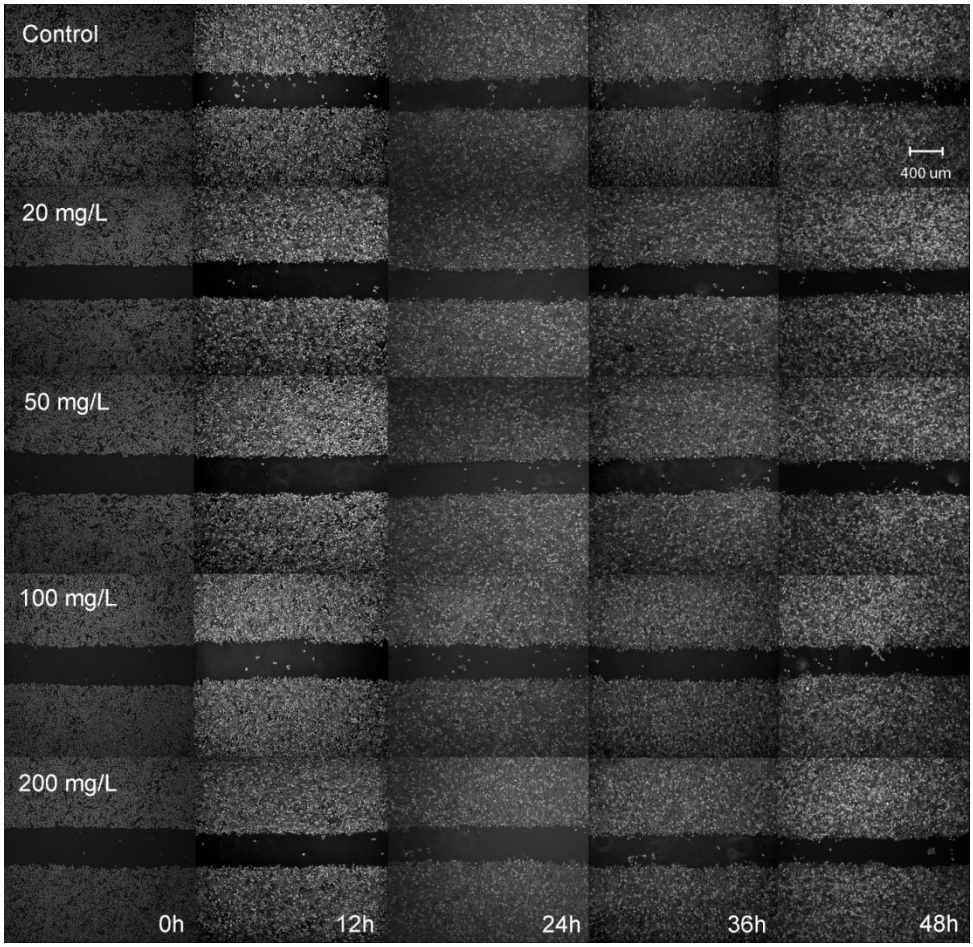

Figure 3. Scratch assay images taken at 12 hour intervals after initial wound are compiled above. TScratch analyzed percent of wound healing at a sensitivity threshold of 0.25. A qualitative observation suggests that decreasing numbers of cells migrated across the wound as PDTC dosage concentrations increased.

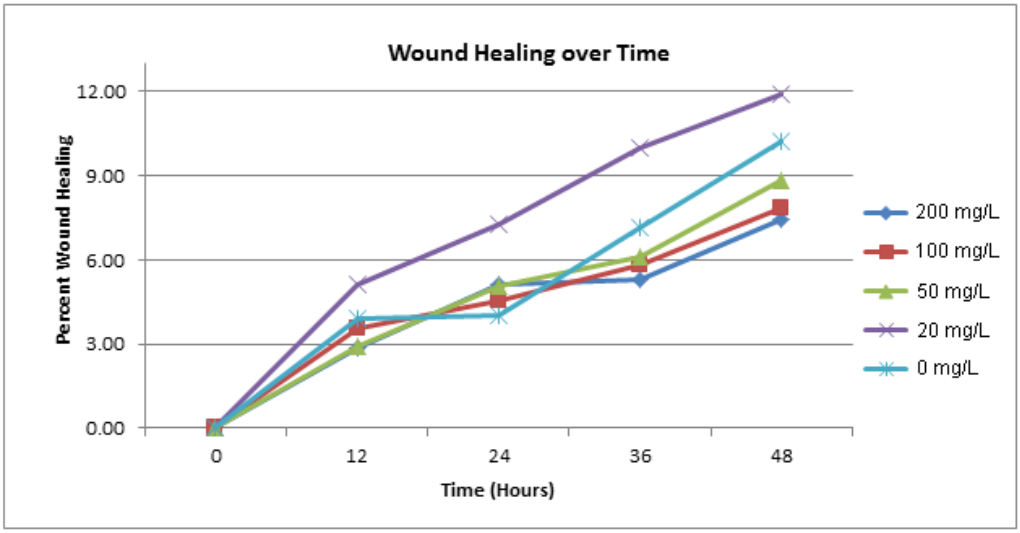

Figure 4. A line graph was constructed to demonstrate percent of wound healing at various time points. Surprisingly, the 20 mg/L PDTC group showed the highest rate of wound healing, which may be explained by the fact that there exists an optimal dosage at which PDTC does not affect EMT or migration.

An ANOVA test for residuals from a line of best fit for each experimental group returned a p-value of 0.002. With an alpha significance level set at 0.05, we are therefore able to reject the null hypothesis that all regression lines were identical, thus concluding that the line of best fine for reach experimental group was distinct. This conclusion was essential to supporting our hypothesis by confirming that varying PDTC concentration was a significant factor in cell migration. However, while we were able to conclude that PDTC had a minimal effect on cell migration, the extent and direction of this inhibition remains unknown. Surprisingly, as shown in Figure 4, the 20 mg/L PDTC dosage group demonstrated the highest rate of wound healing, suggesting that there may be an optimal dosage of PDTC that is correlated with greater migratory ability. However, we must repeat the procedure several more times to confirm this finding.

Western Blot: PDTC did not significantly modulate CCR7 and other EMT markers

Western blot analysis demonstrated that there was no statistically significant modulation among EMT markers, with the exception of N-cadherin in the 24 hour group. After analyzing the images with ImageLab, a linear regression was run on the relative expression of each marker as compared to the control group for each marker. Correlation coefficients and p-values were subsequently retrieved to determine whether there existed any trend among the markers or a relationship between the markers and the amount of PDTC added to each group. Histograms of relative expression of each marker in both time groups are provided in the supplementary figures section at the end of this paper, but a table summary of their p-values are provided below:

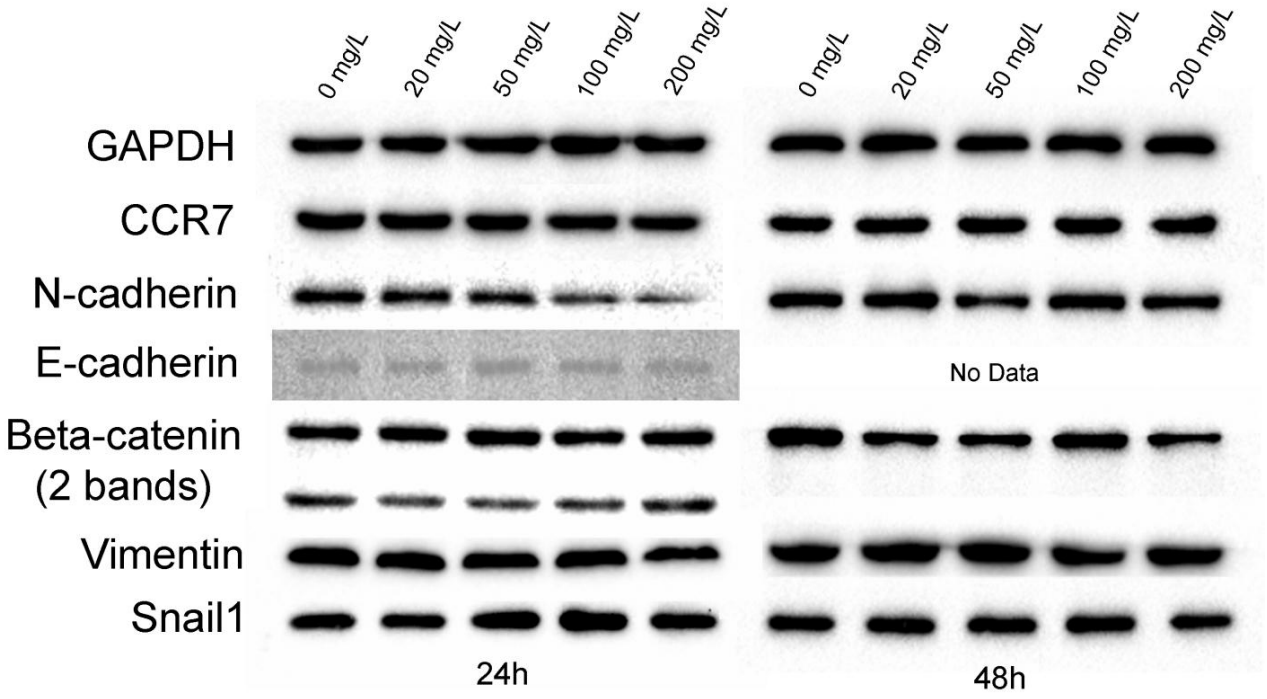

Figure 5. Compiled images of Western blots for both time groups are arranged above. For the 48h time group, E-cadherin was not analyzed (due to time constraints). While β-catenin typically shows up as two bands as demonstrated in the 24h group, it only showed up as one band for the 48h group. At a glance, most markers demonstrate relative consistency in both time groups with the exception of N-cadherin in the 24h group.

	Marker	Slope	Correlation Coefficient	p-value for Independence	z-test for Ho: β=0	p-value for Ho: β=0
24h	GAPDH	0.000314	0.8461	0.2220	0.80092	0.4231
	CCR7	-0.00081	-0.9245	0.1487	-1.4555	0.1455
	N-cadherin	-0.00325	-0.9843	0.0656	**-3.0062**	**0.0026**
	E-cadherin	-5.7E-05	-0.02114	0.9766	-0.02073	0.9834
	Beta-catenin	0.00204	0.3100	0.6726	0.1069	0.9148
	Vimentin	0.00112	0.6254	0.397	0.2678	0.7888
	Snail1	-0.00192	-0.7465	0.3025	-0.4147	0.6783
48h	GAPDH	-0.00026	-0.2434	0.7389	-0.1490	0.8815
	CCR7	-0.0006	-0.4114	0.5774	-0.2421	0.8086
	N-cadherin	0.00075	0.5272	0.4770	0.1917	0.8479
	E-cadherin	N/A	N/A	N/A	N/A	N/A
	Beta-catenin	0.00500	0.6835	0.3517	0.3712	0.7104
	Vimentin	-0.00156	-0.7787	0.2771	-0.7192	0.4719
	Snail1	0.000214	0.07523	0.9172	0.03355	0.9732

Table 1. Relative expression levels of each marker as compared to the control group were analyzed by ImageLab. Relative concentrations were set against the control band for each marker and then divided by the relative expressions of GAPDH at each PDTC concentration accordingly. After running a linear regression, a z-statistic test was subsequently performed to calculate whether the slopes produced by the linear regressions were significant. P-values were obtained from the linear regression, and then evaluated for significance with an alpha significance level set at 0.05.

With an alpha significance level set at 0.05, we failed to reject the null hypothesis that the markers were not modulated, and thus were unable to conclude whether there existed a linear relationship between the amount of PDTC added and the relative expression levels of each EMT marker. A z-statistic analysis also found that the slopes were insignificant with a significance level set at abs [1.75] (with the exception of N-cadherin in the 24h group). While N-cadherin was significantly modulated in the 24h group, this trend was not observed in the 48h group. This may be due to the fact that N-cadherin is one of the very first markers that is upregulated at the onset of EMT, and thus would show more pronounced change in the 24h group (Wang et al. 2013). Our expectations were that E-cadherin expression levels would increase as PDTC dosage concentrations increased and that CCR7, N-cadherin, β-catenin, vimentin, and Snail1 would decrease. The fact that CCR7 and standard EMT markers were not significantly modulated suggests that PDTC was not an effective inhibitor. This lack of inhibition may be due to the absence of a ligand competing with PDTC to bind to CCR7. Without a ligand, the CCR7 signaling pathway may not have been active in the first place. Further discussion about protein-ligand binding is located in the conclusion.

IHC: CCR7+ tumor cells proliferate in tumor samples versus non-tumor samples

Clinical gastric adenocarcinoma samples were first classified as being in stage I, II, III, or IV cancer progression. For statistical analysis, landmarks were placed on all CCR7+ cells on 5 randomly selected images from each sample. Green landmarks were placed on CCR7+ immune cells while red landmarks were placed on CCR7+ tumor cells (Figure 6). CCR7+ immune cells were determined by the roundness of the nucleus and the low nucleus to cytoplasm ratio while CCR7+ tumor cells were determined by the irregular shape and size of the nucleus and the high nucleus to cytoplasm ratio.

After counting the total number of red and green landmarks for each sample, IBM SPSS Statistics 20 software was used for the statistical component of our IHC assay. The method specifically used was the Mann-Whitney U test, and GraphPad Prism 5 was utilized to construct graphical figures.

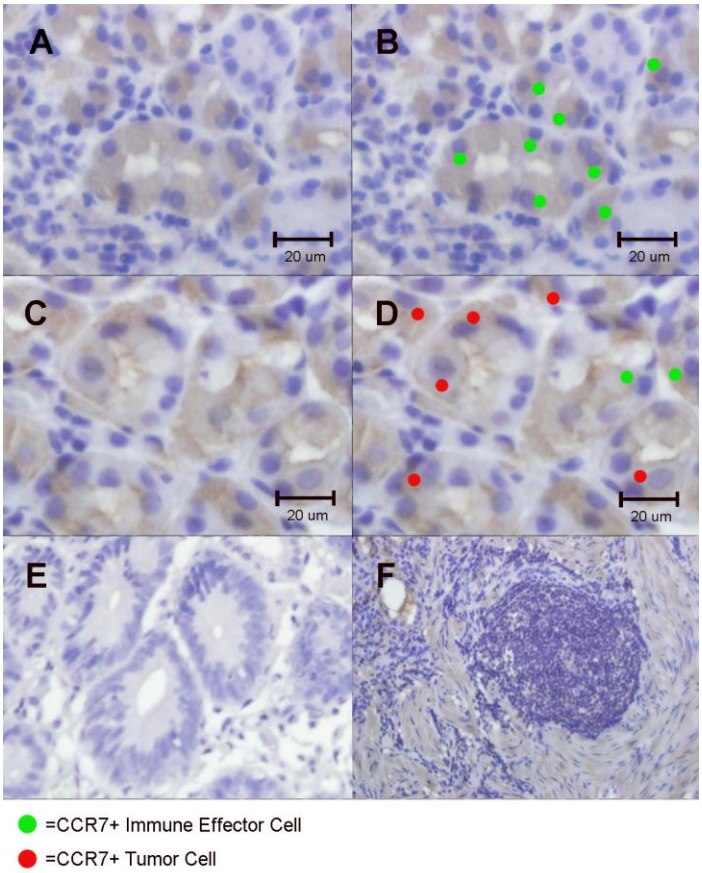

Figure 6. (A) Non-tumor sample; brown staining indicates CCR7 expression while violet circles pinpoint nuclei. CCR7+ cells can be observed as clustering in circular rings. (B) Green landmarks are placed on all CCR7+ immune effector cells as determined by nucleus shape and nucleus to cytoplasm ratio. (C) Tumor-sample; CCR7 expression can be noted in brown staining in cytoplasm and surfaces of cells. Again, CCR7+ cells are observed as clustering in circular rings. (D) Red landmarks are placed on all CCR7+ tumor cells and green landmarks are placed on all CCR7+ immune effector cells. Tumor cells were identified by the irregular size and shape of the nucleus. It is important to note the ratio of tumor to immune cells in the tumor sample. (E) Negative control; no primary antibody was added to the negative controls. As such, no brown staining is observed in the image. (F) Lymph node; lymph nodes are identified by the dense clusters of nuclei surrounded by regions of high CCR7 expression. This highlights CCR7's role in directing cell migration towards lymph nodes.

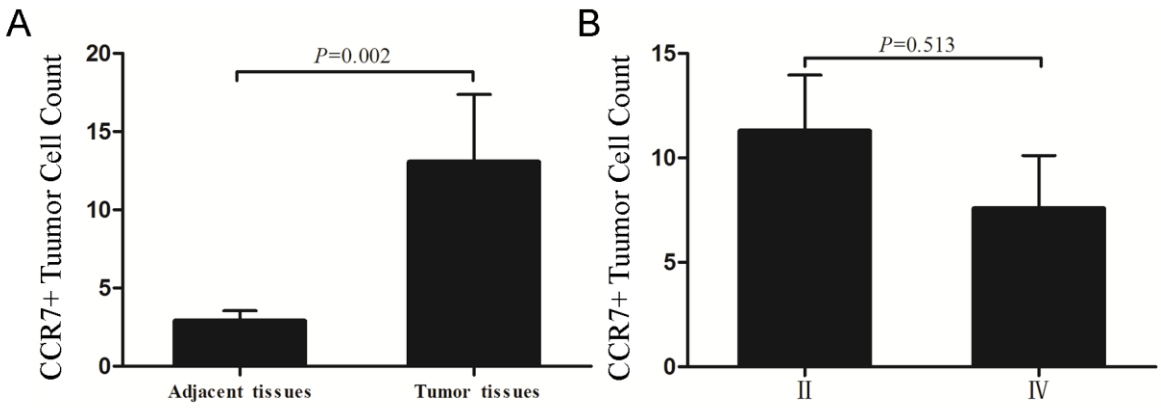

Figure 7. A Mann-Whitney U test was performed to evaluate the number of CCR7+ cells in non-tumor and tumor samples as well as the number of cancerous CCR7+ cells in stage II and IV samples. Due to lack of sufficient samples, stage I and III samples were excluded from the analysis. P-values for (A) and (B) for differences between groups were obtained at 0.002 and 0.513, respectively.

From *Figure 7*, a p-value of 0.002 indicated that there was a significant difference in CCR7+ cancerous cell counts between adjacent (non-tumor) tissues and tumor tissues. This supported our hypothesis that CCR7 is implicated in EMT, since we would have expected high levels of CCR7 expression in tumor cells migrating towards the lymph nodes. However, for between group analyses, because there were not enough samples in stage I and III groups, only samples classified in stage I and IV were analyzed. However, with a p-value of 0.513, we concluded that there was no significant difference in CCR7+ cells between these two stages. This may be due to the small number of samples collected for each stage. Ideally, we would expect that as cancer progresses, there would be increasing numbers of CCR7+ cancerous cells in tumor tissues.

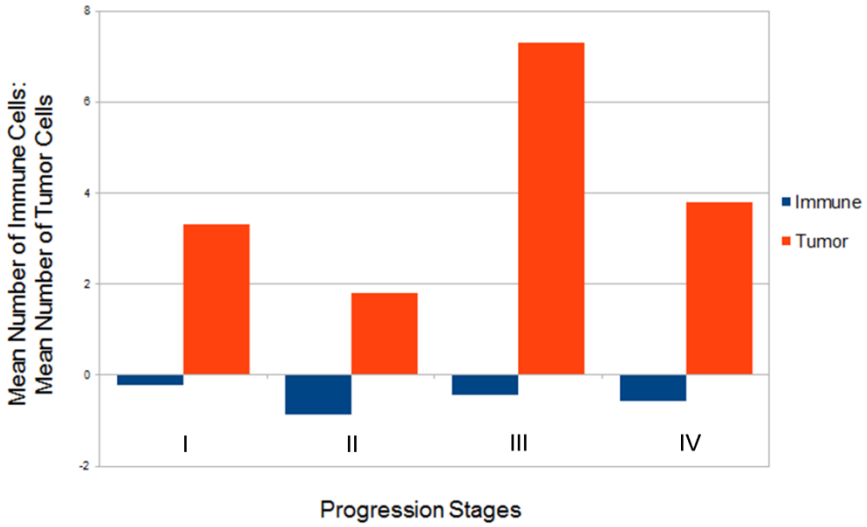

Figure 8. Bar graph illustrating different ratios of mean number of mean immune cells to mean number of tumor cells in samples for each stage. Stage III demonstrated the starkest contrast between tumor and immune cells. This trend, however, may be severely affected by the number of samples analyzed in our experiment.

A separate mean and standard deviation statistical analysis was performed for samples in all four stages. To compensate for small sample numbers, a pooled mean was calculated by taking the mean counts for each sample and then averaging those values. Each value was then further subtracted by 1 to illustrate decreases in number of immune cells. Figure 8 illustrates ratio comparisons between samples at different cancer progression stages. Stage III samples demonstrated the starkest contrast between mean number of immune cells and mean number of tumor cells. Ideally, we would expect a gradual increase in CCR7+ tumor cells as cancer progressed, and a gradual decrease in CCR7+ immune cells as cancer progressed. This would demonstrate the increasingly metastatic nature of each stage. Overall, however, our IHC assay results support our hypothesis that proliferation of CCR7+ tumor cells are increased as gastric cancer metastasizes.

Conclusion

Data from our western blot assay suggest that PDTC may not have been an effective inhibitor of CCR7 in our experiments. This may be due to the reason that no additional ligand was added. PDTC had not been used by our lab before to inhibit CCR7, and we were not certain that it would. By the time we finished performing and analyzing all of our data, we suspected that PDTC did not inhibit CCR7 at all, which explains the similarity in relative expression of all EMT markers across the board. CCR7 itself was not significantly modulated either.

For future research, we would have liked to use PDTC as an inhibitor in combination with one of CCR7's ligand, CCL21. For this project, we assumed that a certain amount of CCL21 was already present in the cells, though in reality, it may not have been a significant amount. In Zhou et al.'s (2010) research, PDTC was shown to suppress CCR7 expression, but only in the presence of SLC. Due to the fact that no initial ligand was added to the experimental groups, there exists the possibility that CCR7 was completely unaffected by the addition of PDTC. We must take into consideration the constant of dissociation formula,

$$Kd = \frac{[P][L]}{[C]}$$

where P represents protein concentration, L represents ligand concentration, and C represents protein-ligand complex. If there was an insignificant level of ligand present in the cells, then the constant of dissociation would automatically return a value of zero, in which we can naturally assume that PDTC was unable to inhibit the CCR7 signaling pathway at all.

In an ideal situation, we would have assumed that PDTC was an effective inhibitor of CCR7 and that enough CCL21 was present in the cells initially for CCR7 to be inhibited. We would then expect that increasing concentrations of PDTC would then accordingly inhibit CCR7 expression at increasing levels. If we were then to test our hypothesis of whether CCR7 is correlated with inducing EMT in gastric carcinoma cells, we would perform various assays to measure the behavioral and molecular characteristics of cells that present with differing levels of CCR7 expression as described previously. Given more time and resources, we would also have liked to perform a transwell assay to quantify the invasiveness of the cells.

If CCR7 proves to be a powerful inducer of EMT in gastric carcinoma cells, future research can focus on blocking or suppressing the CCR7 signaling pathway to delay metastasis in cancer patients. Further inquiry should also be made to determine whether induced EMT promotes CCR7 expression or whether CCR7 expression induces EMT. In addition, other signaling pathways implicated in cell migration should be studied simultaneously to determine if CCR7 interacts with these different receptors to promote EMT. Another way to study the causative effect, if there exists one, between CCR7 and EMT involves genetically engineering a gastric carcinoma cell line to stop expressing CCR7. Known inducers of EMT, such as TGFβ1, are then used to induce EMT. If EMT is not induced in the cells, as established by western blotting and other assays, then CCR7 may be then established as an important instigator of EMT and cancer metastasis. In short, further work should be done to determine if there exists a causative relationship between CCR7 and induced EMT, not just a correlative relationship.

References

Carl-McGrath, Stacy, Matthias Ebert, and Christoph Rocken. "Gastric adenocarcinoma: epidemiology, pathology and pathogenesis." *Cancer Therapy* 5 (2007): 877-894.

Crew, Katherine D, and Alfred I Neugut. "Epidemiology of gastric cancer." *World Journal of Gastroenterology* 12.3 (2006): 354-362.

Maier, Harald J, Uta Schmidt-Strassburger, Margit A Huber, Eva M Wiedemann, Hartmut Beug, and Thomas Wirth. "NF-kB promotes epithelial-mesenchymal transition, migration and invasion of pancreatic carcinoma cells." *Cancer Letters* 295 (2010): 214-228.

Mashino, K., Sadanaga, N., Yamaguchi, H., Tanaka, F., Ohta, M., Shibuta, K., Inoue, H., & Mori, M. (2002). Expression of chemokine receptor CCR7 is associated with lymph node metastasis of gastric carcinoma. *Cancer Research, 62*, 2937-2941.

Lee HJ, Yang HK, Ahn YO. (2002) Gastric cancer in Korea. Gastric Cancer, 5,177–182.

Kwak, M.K, K Hur, D.J Park, Hee J. Lee, H.S Lee, W.H Kim, K.U Lee, K.J Choe, and H.K Yang. "Expression of Chemokine Receptors in Human Gastric Cancer." *Tumor Biology* 26 (2005): 65-70.

Slowik, Guy. "Stomach Cancer - What Are The Stages Of Stomach Cancer?." *ehealthMD*. N.p., 24 Apr. 2012. Web. 1 Aug. 2013.
<http://ehealthmd.com/content/what-are-stages-stomach-cancer#axzz2bRjp52Rg>.

Wang, W., Chen, Y., & Zhang, Y. (2013). The regulatory mechanism of CCR7 expression and its involvement in the metastasis and progression of gastric cancer. *Tumor Biology, 34*, 1865-1871.

Xu, J., Lamouille, S., & Derynck, R. (2009). TGF-β-induced epithelial to mesenchymal transition. *Cell Research, 19*, 156-172.

Zhou, Shuang, Rilun Li, Jie Qin, Cuiping Zhong, and Chunmin Liang. "SLC/CCR7 Stimulates the Proliferation of BMDCs by the pNF-kB p65 Pathway." *The Anatomical Record* 293 (2010): 48-54.

Lab Journal

Week 1
Dr. Ma gave us a brief tour of the lab before walking us through the full procedure of culturing cells. Alex and I were then allowed to go through the entire procedure ourselves so that we could later culture cells on our own. We also learned how to prepare basic solutions that we would be using on later in our experiments.

Week 2
Dr. Ma walked us through the procedure of Western blotting before allowing each of us to perform one on our own on previously isolated proteins from a past experiment. Alex and I also observed a lab technician operate a tissue sectioning machine on brain tissue samples from mice.

Week 3
Xiao Ma introduced IHC to us, and taught us the entire 2-day procedure before allowing Alex and I to do it on our own. Alex and I both did 3 rounds of practice IHC spanning six days. We also surgically retrieved lymph nodes from mice for another lab's project.

Week 4
We continued to practice and change the protocol for IHC. We then did two rounds of official IHC that we analyzed for our report. In addition, we created a control group for our IHC assay.

Week 5
After dividing my AGS cells into different wells/plates, I then treated them with varying concentrations of PDTC. Two days later, we performed a scratch assay and imaged scratch, morphology, and IHC pictures for the rest of the week. At the end of the week, we harvested proteins from our respective cell lines.

Week 6
Due to limited lab supplies, Alex and I had to rotate performing our western blots on each of our cell lines. For my AGS cell line, we did a western blot for CCR7, N-cadherin, and E-cadherin. I also started analyzing my data for my scratch and morphology assays.

Week 7
I continued to perform western blots for our remaining experimental groups and markers. Since lab materials were shared among multiple labs in the building, I would arrive on campus at 7am to start my western blots first and rotate materials with the other researchers. Staggering multiple western blots resulted in me staying at lab until 10-11pm in the evening.

Week 8
During this final week, we pushed to finish up our last experiments, including western blot and IHC statistical analysis. Due to time constraints, we could no longer perform our transwell assays that we originally wanted to include in our experiment. I input all of my collected data into excel and various other analysis software and created figures and graphs for my paper. Everything was done on MorphoJ, TScratch, Microsoft Excel, and ImagLab. Alex and I also presented our final paper to the lab on Thursday.

Supplementary Figures

Time Group	Marker	Amount PDTC Treatment (mg/L)				
		0	20	50	100	200
24h	GAPDH	1	1.03	1.04	1.02	1.08
	CCR7	1	1.00	1.03	0.95	0.85
	N-cadherin	1	0.85	0.76	0.56	0.32
	E-cadherin	1	0.98	0.74	0.53	1.03
	Beta-catenin	1	1.85	1.44	1.43	1.44
	Vimentin	1	1.32	1.24	1.32	1.34
	Snail	1	1.27	1.09	0.79	0.79
48h	GAPDH	1	0.96	0.85	1.06	0.89
	CCR7	1	1.10	1.24	0.95	0.98
	N-cadherin	1	1.23	1.00	1.12	1.22
	E-cadherin	N/A	N/A	N/A	N/A	N/A
	Beta-catenin	1	1.92	1.44	1.20	2.45
	Vimentin	1	0.99	1.16	0.96	0.72
	Snail	1	1.46	1.60	1.25	1.30

Supplementary Figure 1. Relative expression levels of all EMT markers tested.

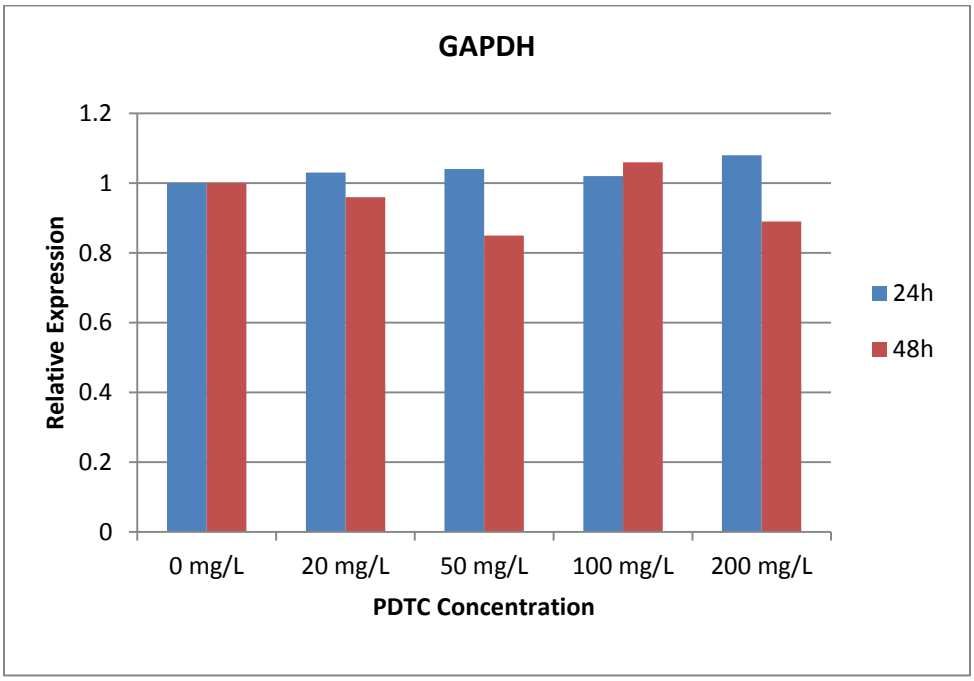

Supplementary Figure 2. Bar graph detailing GAPDH expression levels in both the 24h and 48h groups.

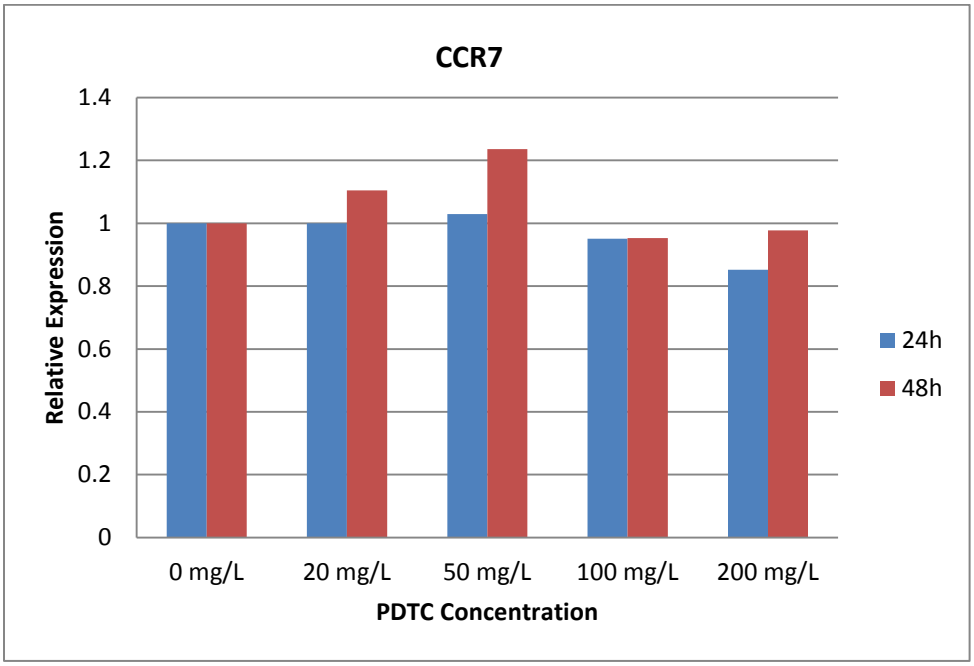

Supplementary Figure 3. Bar graph detailing CCR7 expression levels in both the 24h and 48h groups.

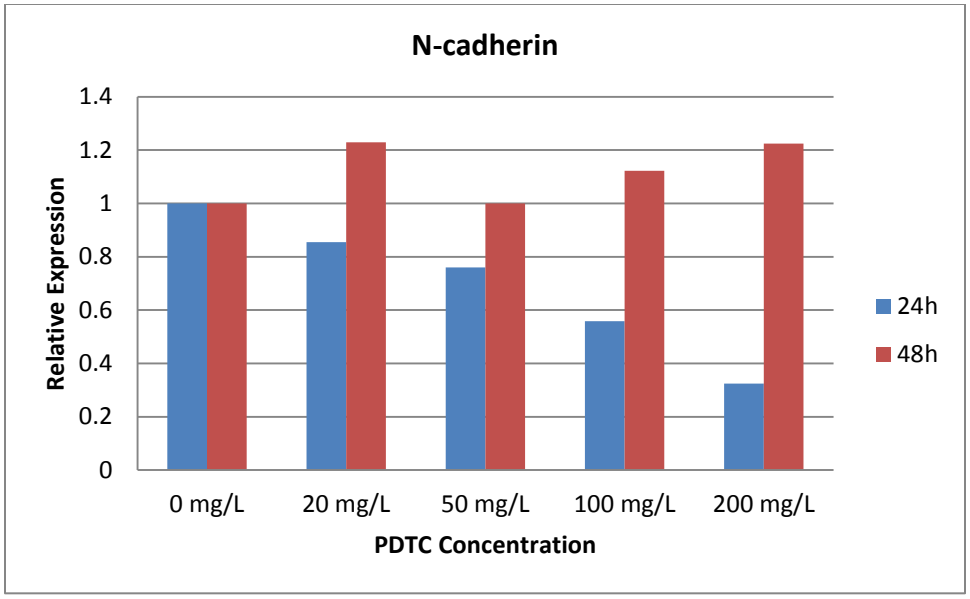

Supplementary Figure 4. Bar graph detailing N-cadherin expression levels in both the 24h and 48h groups.

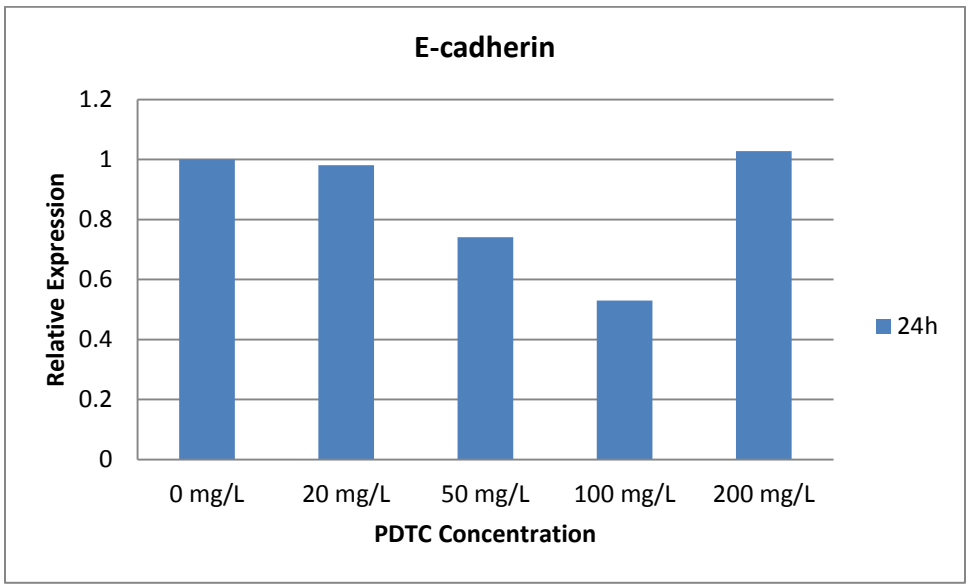

Supplementary Figure 5. Bar graph detailing E-cadherin expression levels in both the 24h and 48h groups.

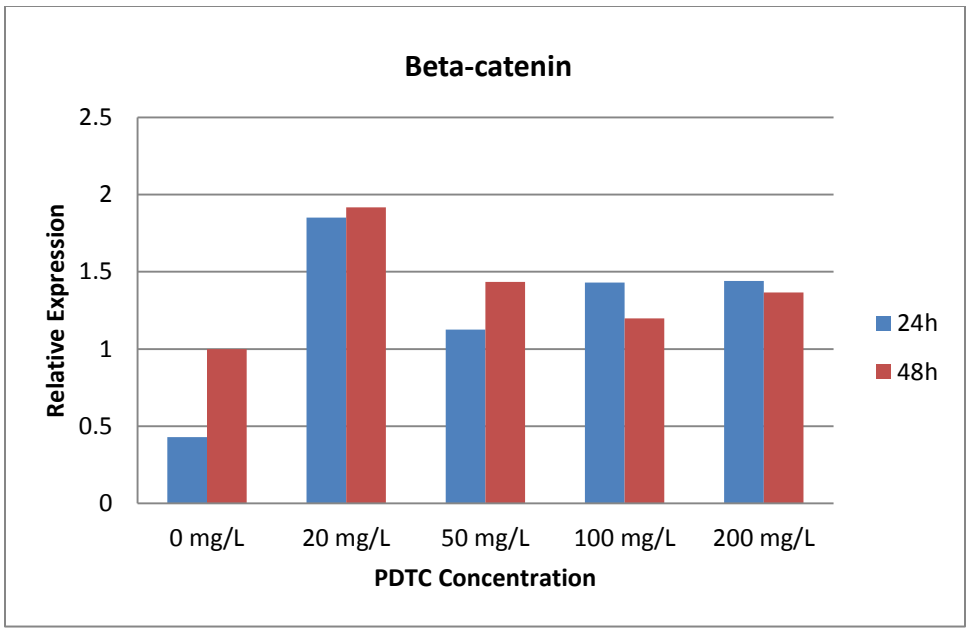

Supplementary Figure 6. Bar graph detailing Beta-catenin expression levels in both the 24h and 48h groups.

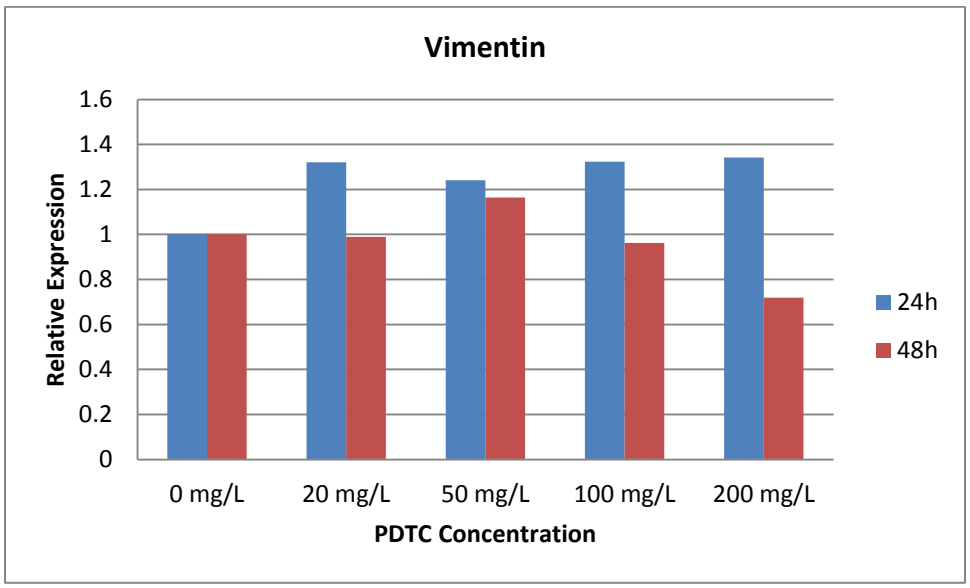

Supplementary Figure 7. Bar graph detailing Vimentin expression levels in both the 24h and 48h groups.

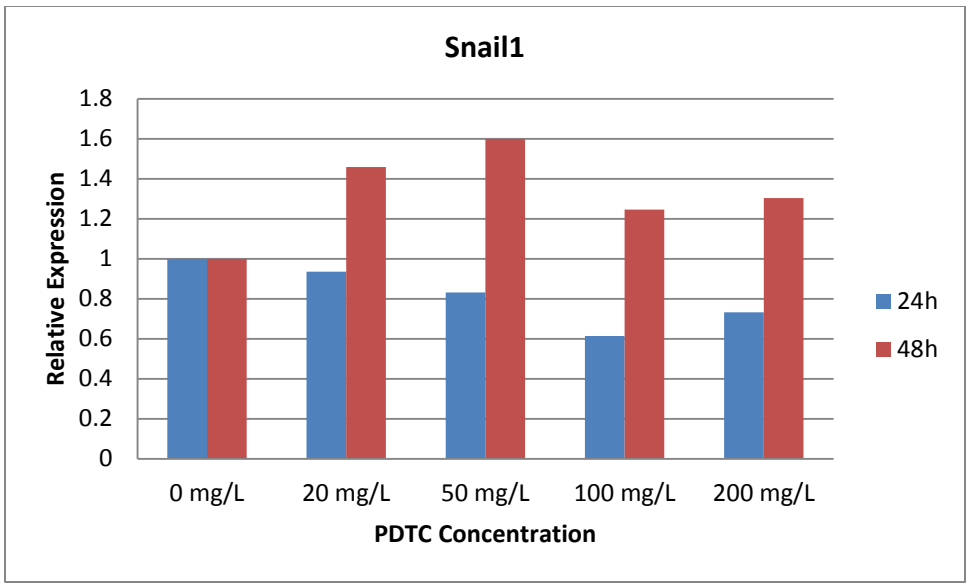

Supplementary Figure 8. Bar graph detailing Snail1 expression levels in both the 24h and 48h groups.

	Time				
	0h	12h	24h	36h	48h
0 mg/L	0	2.87	5.1	5.3	7.45
20 mg/L	0	3.57	4.56	5.84	7.83
50 mg/L	0	2.94	5.06	6.09	8.81
100 mg/L	0	5.13	7.27	10	11.88
200 mg/L	0	3.89	4.04	7.13	10.22

Supplementary Figure 9. Table of percent wound-healing values scratch assay are arranged above.